A nonlinear texture operator specialised in the analysis of dot-patterns

Kruizinga, P.; Petkov, N.

Published in:
15TH INTERNATIONAL CONFERENCE ON PATTERN RECOGNITION, VOL 1, PROCEEDINGS

Publication date:
2000

A nonlinear texture operator specialised in the analysis of dot-patterns

P. Kruizinga and N. Petkov
Institute of Mathematics and Computing Science, University of Groningen
P.O. Box 800, 9700 AV Groningen, The Netherlands
peterkr@cs.rug.nl, petkov@cs.rug.nl

Abstract

The performance of two well-known texture operators (based on Gabor energy and the cooccurrence matrix) is compared with the performance of a new, biologically motivated texture operator, the dot-pattern selective cell operator. The comparison is made using a quantitative method based on the Mahalanobis distance. Together with some classification experiments the comparison shows a clear superiority of the new operator in dot-pattern texture problems.

1. Introduction

Neurophysiologists discovered cells in the visual cortex of monkeys that responded exclusively to dot-patterns [10]. Elsewhere we proposed a computational model of this type of cell and demonstrated that it is capable of reproducing the results of neurophysiological experiments [6, 7]. In this paper we use this model as a basis of an image processing operator that we call the dot-pattern selective cell operator. We show that this operator is specifically effective in processing dot-pattern texture. The features extracted with it are compared with commonly used texture features obtained with cooccurrence matrix and Gabor energy operators. For this comparison we use the Mahalanobis distance between clusters of feature vectors derived from different types of texture [4, 5]. This method enables a quantitative evaluation of the texture discrimination properties of feature extraction operators. The method differs from the commonly used texture feature performance evaluation method which is based on the comparison of classification results [1, 8, 9, 11]. The problem with the traditional comparison method is that it mixes together the discrimination properties of the feature extraction operator with the performance of a classifier. In our method, the discrimination properties of the feature extraction operator can be separated from the performance of a subsequent classifier. For completeness, we use the features obtained with the dot-pattern selective cell operator also in segmentation experiments and compare the results with the results achieved with Gabor energy and cooccurrence matrix features.

2. Spot detector model

Though most of the cells in the primary visual cortex (V1) are orientation selective, about 10-20% of the cells do not show any orientation preference. Most of these 'centre-surround cells' have a receptive field profile which can be modelled by means of a Difference-of-Gaussians (DoG) function as follows:

$$u_{\xi,\eta,\sigma,\gamma}(x,y) = \frac{1}{2\pi\sigma^2}\left(\frac{1}{\gamma^2}e^{-\frac{(x-\xi)^2+(y-\eta)^2}{2\gamma^2\sigma^2}} - e^{-\frac{(x-\xi)^2+(y-\eta)^2}{2\sigma^2}}\right) \quad (1)$$

where x and y specify the position of a light impulse in the visual field and ξ, η, σ and γ are parameters as follows:

The centre of the receptive field within the visual field is specified by the pair (ξ, η). The parameters σ and γ specify the standard deviations $\sigma_c = \gamma\sigma$ $(\gamma < 1.0)$ and $\sigma_s = \sigma$ of the centre and the surround Gaussians, respectively. In our experiments we used a value of $\gamma = 0.5$. The normalisation factor $\frac{1}{\gamma^2}$ in front of the centre Gaussian is used to obtain a function with a zero DC component. With this value of γ, the radius of the central region r_σ is approximately equal to σ: $r_\sigma = 0.96\sigma$. In our experiments we used two types of spot detectors: one with a positive (excitatory), and the other with a negative (inhibitory) central region. These cells are modelled by a two-stage model consisting of a first, linear filtering stage and a second, non-linear stage which includes thresholding and contrast normalisation. The linear stage consists in computing an integral

$$s_{\xi,\eta,\sigma,\gamma} = \iint f(x,y)u_{\xi,\eta,\sigma,\gamma}(x,y)\mathrm{d}x\mathrm{d}y \quad (2)$$

where $f(x,y)$ is the intensity distribution of an input image. In the second stage, contrast normalisation is performed by

0-7695-0750-6/00 $10.00 © 2000 IEEE

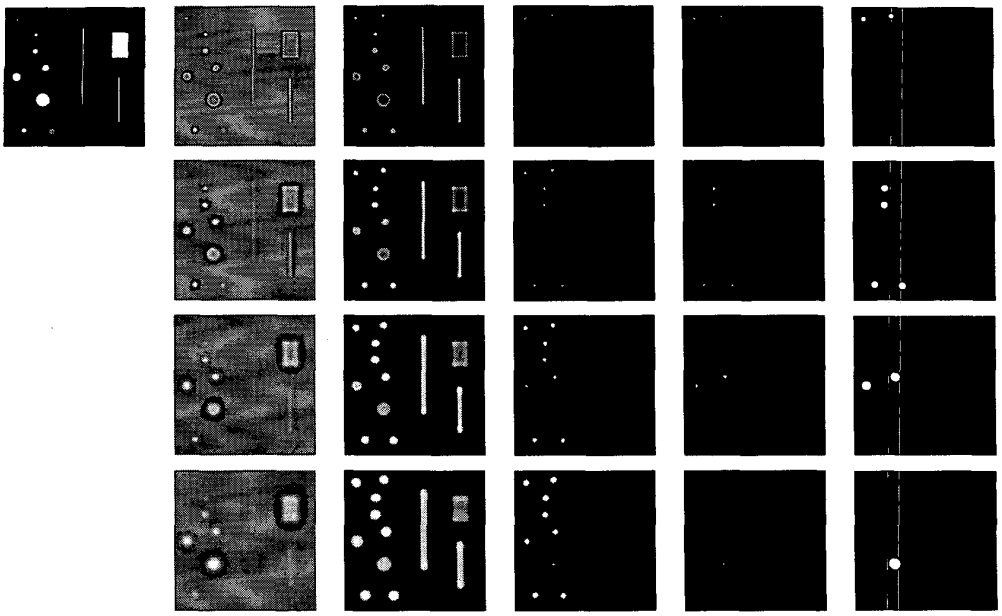

Figure 1. The single image in top-left position is a synthetic input image, which includes features of different form, size and contrast. Each row in the 4×5 block of images corresponds to an operator tuned to a given optimal size of the spots to be detected. The images in the first column are the results of convolutions with centre-surround receptive field functions of four different sizes (a). The results which are normalised for contrast are shown in the second column (b). The effect of lateral inhibition and winner-take-all competition on the responses of spot detecting subunits are illustrated by the third (c) and fourth (d) columns, respectively. For illustration purposes, in the fifth, rightmost column (e), the responses of the spot detecting subunits shown in (d) are replaced by the corresponding optimal size stimuli.

dividing the linear response $s_{\xi,\eta,\sigma,\gamma}$ by the weighted average gray level of the image within the receptive field of the modelled cell. The weighted average gray level $a_{\xi,\eta,\sigma}$ is computed as follows:

$$a_{\xi,\eta,\sigma} = \frac{1}{2\pi\sigma^2} \iint f(x,y) e^{-\frac{(x-\xi)^2+(y-\eta)^2}{2\sigma^2}} \mathrm{d}x\mathrm{d}y \qquad (3)$$

In order to implement contrast normalisation, we use the hyperbolic ratio function to calculate the output of the centre-surround cell from the ratio $l_{\xi,\eta,\sigma,\gamma} = \frac{s_{\xi,\eta,\sigma,\gamma}}{a_{\xi,\eta,\sigma}}$ which is proportional to the local contrast within the receptive field of the cell:

$$v_{\xi,\eta,\sigma,\gamma} = \begin{cases} 0 & \text{if } a_{\xi,\eta,\sigma} = 0 \\ \chi\left(\frac{l_{\xi,\eta,\sigma,\gamma} R}{l_{\xi,\eta,\sigma,\gamma} + C}\right) & \text{otherwise} \end{cases} \qquad (4)$$

where $\chi(z) = 0$ for $z < 0$, $\chi(z) = z$ for $z \geq 0$ (thresholding) and R and C are the maximum response level and the semi-saturation constant, respectively.

The modelled centre-surround cell will react strongly to a light spot which is located entirely in the centre, excitatory region of the receptive field, though the cell will also react to other features in its receptive field such as lines or edges. The function of an ideal spot detector is, however, to signal spots only. Our computational model of spot detectors is based on a lateral inhibition mechanism. A spot detecting subunit $v'_{\xi,\eta,\sigma,\gamma}$ gets its input from the modelled centre-surround cell $v_{\xi,\eta,\sigma,\gamma}$ and a number of nearby similar cells with the same preferred spot size. The concerned subunit has the same output as the centre-surround cell with the same location (ξ, η) if the nearby cells show no response. Other image features may also invoke a reaction of the cell, but they will cause a reaction of nearby cells as well. In that case, the output of the spot detecting subunit $v'_{\xi,\eta,\sigma,\gamma}$ is influenced by the outputs of nearby centre-surround cells in such a way that, if at least one of these cells reacts, the subunit response is suppressed, *i.e.* the response is set to

zero. In our model the lateral inhibition scheme involves a fixed number of nearby centre-surround cells lying in a circle around the centre of the receptive field (ξ, η):

$$v'_{\xi,\eta,\sigma,\gamma} = \begin{cases} v_{\xi,\eta,\sigma,\gamma} & \text{if } \forall i,\ i \in \{1..N\}, \\ & v_{\xi+\Delta\xi_i,\eta+\Delta\eta_i,\sigma,\gamma} < \rho v_{\xi,\eta,\sigma,\gamma} \\ 0 & \text{otherwise} \end{cases} \tag{5}$$

$$\Delta\xi_i = R_{lat} \cos\left(\frac{2\pi i}{N}\right),\ \Delta\eta_i = R_{lat} \sin\left(\frac{2\pi i}{N}\right) \tag{6}$$

where ρ is a fixed factor (in our experiments we used $\rho = 0.8$) and R_{lat} is the distance between the centre of the considered cell and the nearby cells. We choose $R_{lat} = 1.36\sigma$. The number of nearby cells that are involved in the inhibition process is set to $N = 15$. This value is high enough to guarantee that the spot detectors do not react to features other than spots.

In our experiments we use spot detecting subunits with different values of σ to achieve detection of spots on different scales. This introduces a coding redundancy since spot detecting subunits on more than one scale, but with receptive fields centred at the same position, will react to a spot in their receptive field. This redundancy can be eliminated by suppressing all outputs of non-optimal spot detecting subunits at the same position. This is implemented by a winner-takes-all mechanism across all subunits with the same receptive field centre but with different values of the size parameter σ. The ultimate response of a spot detecting subunit $\tilde{v}_{\xi,\eta,\sigma,\gamma}$ is computed as follows:

$$\tilde{v}_{\xi,\eta,\sigma,\gamma} = \begin{cases} v'_{\xi,\eta,\sigma,\gamma} & \text{if } v'_{\xi,\eta,\sigma,\gamma} = \max(v'_{\xi,\eta,\sigma',\gamma} | \forall\, \sigma') \\ 0 & \text{otherwise} \end{cases} \tag{7}$$

The winner-takes-all mechanism will cause the information concerning the location of spots in the image to be separated into different channels, depending on the size of the spots. The sensitivity of the dot-pattern selective cells to spots with different sizes will therefore depend on the sampling on the scale-range. In our experiments we used four different scales.

The processing of visual information by this model is illustrated in Fig. 1, together with the results at intermediate stages. The intensity of a pixel in a result image represents the response of the corresponding part of the model with a receptive field centred at that pixel. As can be seen from the intermediate results after convolution of the input image with a centre-surround receptive field function (Fig. 1a), there is a response not only to spots, but also to other image features. At this stage, the strength of the response depends on the local contrast of the features. This dependence is eliminated by the contrast normalisation step (Fig. 1b). The lateral inhibition eliminates the response to non-spot stimuli (Fig. 1c). Finally, the winner-takes-all mechanism across all channels suppresses all responses to sub-optimal spot stimuli and ensures that each spot is detected in one channel only (Fig. 1d)

3 Dot-pattern selective cell model

In the second stage of our model, the outputs of the spot detecting subunits are combined by so-called spot-pattern subunits using an AND-type nonlinearity. In the final stage, the actual dot-pattern selective cells sum the responses of a large number of spot-pattern subunits in the vicinity of their receptive field centre. This means that modelled dot-pattern selective cells will only react if a number of spots with a specific size are present in their receptive fields. The response increases with the number of spots up to a given maximum. This model is next explained in more detail.

The activity of a so-called spot-pattern subunit $t_{\xi,\eta,\sigma,\gamma,\zeta}$ with position (ξ, η) and preferred spot size specified by σ, is calculated as follows:

$$t_{\xi,\eta,\sigma,\gamma,\zeta} = \begin{cases} 1 & \text{if Card}\{\tilde{v}_{\xi+\Delta\xi_i,\eta+\Delta\eta_i,\sigma,\gamma} : \\ & i = 1 \ldots n : \\ & \tilde{v}_{\xi+\Delta\xi_i,\eta+\Delta\eta_i,\sigma,\gamma} > 0\} \geq 3 \\ 0 & \text{otherwise} \end{cases} \tag{8}$$

where the position of the involved spot detecting subunits is taken at random within the neighbourhood of (ξ, η):

$$\begin{aligned} \Delta\xi_i &= \sigma(\zeta + r_i)\cos\alpha_i \\ \Delta\eta_i &= \sigma(\zeta + r_i)\sin\alpha_i\,, \quad i = 1 \ldots n \end{aligned} \tag{9}$$

where $\sigma\zeta$ is a fixed radius (ζ specifies the density of the spots in the pattern) and r_i are random numbers taken from a normal distribution with zero mean and standard deviation 0.5 and α_i are random numbers taken from a uniform distribution between 0 and 2π. The number of locations n which are taken into account in the determination of dot-pattern presence in the receptive field is larger than the number of spots to be detected. In our experiments we set the number of inspected locations to 30. The dot-pattern subunit is activated only, if three or more spots are detected in these 30 locations.

Finally, the response of a dot-pattern cell $b_{\xi,\eta,\sigma,\gamma,\zeta}$, which is centred at position ξ, η in the visual field and has preferred spot size specified by σ, is computed by weighted summation of the dot-pattern subunits:

$$b_{\xi,\eta,\sigma,\gamma,\zeta} = \iint e^{-\frac{(\xi-\xi')^2+(\eta-\eta')^2}{2\beta\sigma^2}} t_{\xi,\eta,\sigma,\gamma,\zeta} \mathrm{d}\xi' \mathrm{d}\eta' \tag{10}$$

Together with σ, the parameter β specifies the size of the region in which the weighted summation takes place. Larger values of β result in a uniform response in a dot-pattern area even with larger discontinuities in the dot pattern. The function of the operator is illustrated in Fig. 2. The operator is available at http://www.cs.rug.nl/~imaging/.

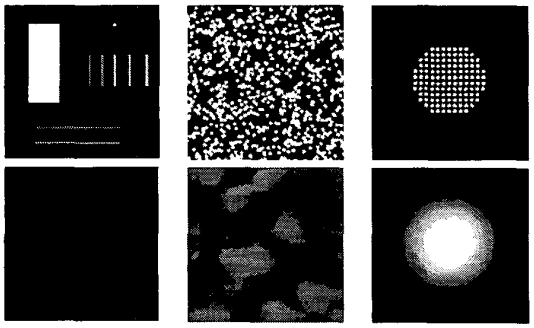

a) b) c)

Figure 2. Input images (upper row) and result images computed by a dot-pattern selective cell operator (lower row). The operator does not react to single dot stimuli and to non-spot image features as lines and edges (a). Irregular dot-patterns of optimal spot size and average density result in a small response (b). The detection capability of dot-pattern selective cell opeartor is illustrated in (c): the operator reacts only in the area filled with a dot-pattern texture.

4. Texture features and the Mahalanobis distance

The quantities computed with a set of dot-pattern selective cell operators can be used as texture features. We next compare the following sets of features:

- **Dot-pattern selective cell features:** A set of dot-pattern selective cell operators with four different preferred spot sizes, three values of the spot density and selective for both black and white spots, is applied to an image, yielding a vector of 24 features in each point.
- **Gabor energy features:** A popular set of texture features is based on the use of Gabor filters [3]. In this case, an image is filtered with a set of Gabor filters with different orientations, spatial frequencies and phases. Using eight orientations and three preferred spatial-frequencies and combining the results of symmetric and anti-symmetric filters, this multi-channel filtering scheme yields a feature vector of 24 Gabor energy quantities [5]. The preferred orientations and spatial-frequencies are chosen in such a way that the filters cover the spatial-frequency domain.
- **Cooccurrence matrix features:** A classic method for texture segmentation is based on the gray-level cooccurrence matrices [2]. In each point of a texture image, a set of gray-level cooccurrence matrices is calculated for different orientations and lengths of the inter-pixel displacement vector. From these matrices, a number of features is extracted which characterise the neighbourhood of the concerned pixel. In our experiments eight gray-level cooccurrence matrices were calculated in each point using a neighbourhood of size 12×12. From each of the matrices three features (energy, inertia and entropy) were extracted, resulting in a vector of 24 features in each image point [5].

The feature vectors computed at different points of a texture image using a given operator are not identical. They rather form a cluster in the multi-dimensional feature space. The larger the distance between two clusters which correspond to two different types of texture, the better the discrimination properties of the texture operator which produced the feature vectors. The distance has, of course, to be related to the (spread) size of the clusters. In order to determine the distance between two clusters of feature vectors, relative to their compactness, we use the Mahalanobis distance

$$D = \sqrt{(\mu_1 - \mu_2)S^{-1}(\mu_1 - \mu_2)} \qquad (11)$$

where μ_1 and μ_2 are the means of the clusters and S is their pooled covariance matrix.

5. Performance evaluation and comparison

The performance of the concerned texture operators is evaluated by measuring the separability of pairs of nine test images, each containing a single dot-pattern texture (parts of these single texture images are used in the composite image shown in Fig. 3a). The separability is measured in the following way: a given vector operator is applied to each image, resulting in a 24-dimensional feature vector field. The pooled covariance matrix is calculated for each pair of images using 1000 sample feature vectors from each image and then the Mahalanobis distance is evaluated according to eq.(11).

Table 1 shows some statistics of the values of the Mahalanobis distance for the three concerned texture operators. The values listed are the minimum, the maximum and the average Mahalanobis distance of all 36 possible pairs of test images. The average Mahalanobis distance for all operators

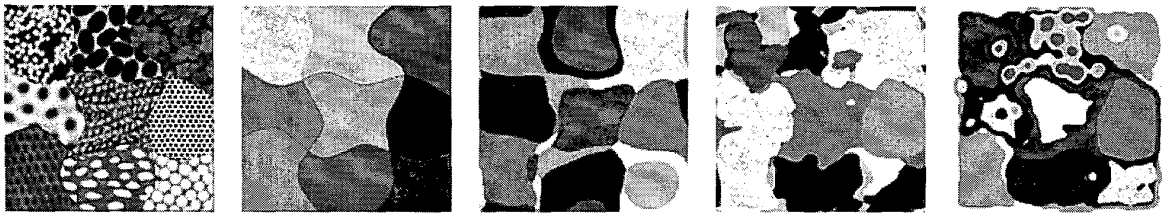

a) b) c) d) e)

Figure 3. An input image containing nine different textures (a) and its exact segmentation (b). The three right-most images show the segmentation results based on the dot-pattern selective cell features (c), the Gabor energy features (d), and the cooccurrence matrix features (e).

is 4.38 or higher. This is enough to enable a linear separation of the textures based of the resulting feature vector fields. The minimum values obtained with the cooccurrence matrix operator and the Gabor energy operator, however, are too small to allow a linear discrimination. The minimum value listed is 1.02, obtained for a certain pair of test images using the Gabor energy features. Assuming normal distribution, this means that for the concerned image pair, the projected feature vector clusters overlap for about 48%, which with certainty does not allow a linear separation of these clusters.

As can be seen from the table, the average Mahalanobis distance between clusters of feature vectors computed with the dot-pattern selective cell operator is three times larger than the average computed with the Gabor energy operator. In turn, the average Mahalanobis distance based on the Gabor energy operator is two times larger than the average obtained with the cooccurrence matrix operator. From these results it may be concluded that the dot-pattern selective cell operator has better discrimination properties with respect to dot-pattern textures than the other two operators.

Table 1. Statistics of the Mahalanobis distance values.

Feature type	Avg	Min	Max
Cooccurrence matrix feat.	4.38	2.40	6.34
Gabor energy feat.	8.83	1.02	32.38
Dot-pattern selective cell feat.	29.51	5.47	159.35

Finally, Fig. 3 shows the results of pixel classification using K-means clustering of the generated feature vectors. The results confirm the comparison results based on the Mahalanobis distance. The dot-pattern selective cell operator clearly has better discrimination and segmentation properties with respect to dot-pattern textures than the other two operators.

References

[1] R. Conners and C. Harlow. A theoretical comparison of texture algorithms. *IEEE Transactions on Pattern Analysis and Machine Intelligence*, 2(3):204–222, 1980.

[2] R. Haralick, K. Shanmugam, and I. Dinstein. Textural features for image classification. *IEEE Transactions on Systems, Man and Cybernetics*, 3(6):610–621, 1973.

[3] A. Jain and F. Farrokhnia. Unsupervised texture segmentation using gabor filters. *Pattern Recognition*, 24(12):1167–1186, 1991.

[4] P. Kruizinga and N. Petkov. Grating cell operator features for oriented texture. In A. Jain, S. Venkatesh, and B. Lovell, editors, *Proc. of the Int. Conf. on Pattern Recognition*, pages 1010–1014, Brisbane Australia, August 16-20 1998.

[5] P. Kruizinga and N. Petkov. Non-linear operator for oriented texture. *IEEE Transactions on Image Processing*, 8(10):1395–1407, 1999.

[6] P. Kruizinga and N. Petkov. Nonlinear operator for blob texture segmentation. In e. a. A.S. Cetin, editor, *Proc. of NSIP'99*, volume II, pages 881–885, Antalya, Turkey, 1999.

[7] P. Kruizinga and N. Petkov. Computational model of dot-pattern selective cells. *Biological Cybernetics*, 2000. In press.

[8] P. Ohanian and R. Dubes. Performance evaluation for four classes of textural features. *Pattern Recognition*, 25(8):819–833, 1992.

[9] O. Pichler, A. Teuner, and B. Hosticka. A comparison of texture feature extraction using adaptive gabor filtering, pyramidal and tree structured wavelet transforms. *Pattern Recognition*, 29(5):733–742, 1996.

[10] K. Tanaka, H. Saito, Y. Fukada, and M. Moriya. Coding visual images of objects in the inferotemporal cortex of the macaque monkey. *Journal of Neurophysiology*, 66(1):170–189, 1991.

[11] Z. Wang, A. Guerriero, and M. Desario. Comparison of several approaches for the segmentation of texture images. *Pattern Recognition Letters*, 17(5):509–521, 1996.